Available online at www.sciencedirect.com
SCIENCE DIRECT®
ELSEVIER
Journal of Nuclear Materials 321 (2003) 177–183
journal of nuclear materials
www.elsevier.com/locate/jnucmat

Influences of laser surface alloying with niobium (Nb) on the corrosion resistance of Zircaloy-4

SungJoon Lee [a], ChanJin Park [a], YunSoo Lim [b], HyukSang Kwon [a,*]

[a] *Department of Materials Science and Engineering, Korea Advanced Institute of Science and Technology, 373-1, KusongDong, YouSongGu, TaeJon 305-701, South Korea*

[b] *Korea Atomic Energy Research Institute, 105, DeokJinDong, YuSongGu, TaeJon 305-353, South Korea*

Received 10 May 2002; accepted 21 April 2003

Abstract

The influence of laser surface alloying (LSA) with niobium (Nb) on the corrosion and mechanical properties of Zircaloy-4 was examined by potentiodynamic polarization test in a chloride solution at 80 °C and immersion test in a steam at 400 °C, and microhardness test. The results are discussed with structural and compositional variations of LSA layer. LSA on the Zircaloy-4 precoated with Nb produced a Nb-alloyed layer 170–300 μm thick with 1.3–2.5 wt% Nb, depending on laser beam power. The alloyed layer was composed of a mixed structure of α-Zr and β-Zr phases with the β-Zr phase being increased with the Nb content in the alloyed layer. Microhardness of Zircaloy-4 was increased by LSA with Nb, due to three factors; solid solution hardening with Nb, grain-size refinement by rapid cooling, and transformed β phase. The significant improvement in the resistance to localized corrosion of laser surface alloyed Zircaloy-4 in a chloride solution was attributed to the combined effects of rapidly cooled fine microstructure and the Nb alloying. However, the corrosion resistance of laser surface alloyed Zircaloy-4 was reduced in steam at 400 °C, a result of the formation of β-Zr phase and Zr hydrides.

PACS: 28.41.Qb; 81.65.−b; 81.65.Kn; 68.55.Ln

1. Introduction

Zirconium alloys have been extensively used as cladding materials for fuel rods in nuclear reactors, due to their low thermal neutron absorption cross-section, excellent corrosion resistance and good mechanical properties at high temperatures. Zircaloy-4 is a specific zirconium based alloy containing, on a weight percent basis, 1.2–1.7% Sn, 0.18–0.24% Fe and 0.07–0.13% Cr, and were developed for use in pressurized water reactors (PWR). Zircaloy-4 tubes, however, have often been reported to be failed by fretting corrosion occurring at the tube-grid contact due to flow-induced assembly vibration and also by erosion (debris-induced fretting) caused by debris such as Fe_3O_4, Fe_2O_3 flowing and moving in coolant [1,2]. Since these corrosion failures result in reduction in life time of the fuel cladding tube as well as contamination of radioactive materials, it is necessary to improve wear and corrosion resistance of fuel cladding.

Alloy developments and surface treatments have been attempted to improve the corrosion and mechanical properties of Zircaloy tube. For the developments of new fuel cladding alloy, intermediate alloys between Zircaloy and Zr–Nb binaries have been actively pursued; E635 (Zr–1.2Sn–1Nb–0.4Fe) in former USSR and ZIRLO (Zr–1Sn–1Nb–0.1Fe) by Westinghouse were developed [3–5]. These alloys were reported to be much less sensitive to corrosion in high temperature water containing high dissolved O_2 as well as high Li

* Corresponding author. Tel.: +82-42 869 3326; fax: +82-42 869 3310.
E-mail address: hskwon@mail.kaist.ac.kr (HS. Kwon).

0022-3115/$ - see front matter © 2003 Elsevier B.V. All rights reserved.
doi:10.1016/S0022-3115(03)00245-9

concentration. Ion implantation [6–8] and laser treatment [9,10] have been applied to modify the surface properties of the Zircaloy tube. The laser surface treatment of metals is a process where a small surface volume of materials is melted instantly by a laser beam and rapidly cooled, thereby producing very fine microstructure with an improved wear and corrosion resistance. Laser surface melting (LSM) was reported to improve the corrosion resistance of Zircaloy-4 in acid solution [9,10]. However, the influence of laser surface alloying (LSA) with Nb or Cr on the corrosion and mechanical properties of Zircaloy-4 has not been studied yet. Research objective of the present study is to form an alloyed layer with Zr–Nb–Sn–Fe–Cr system (analogous to ZIRLO and E635) on a surface of Zircaloy-4 by the LSM technique and to examine the corrosion and mechanical properties of the alloyed layer.

2. Experimental procedure

Zircaloy-4 used in this study was provided in the form of annealed sheet 1.7 mm thick. Its chemical composition is presented in Table 1. Samples with dimensions of 35 mm × 80 mm were cut from the sheet and mechanically polished down to 600 grit SiC paper, then chemically polished in 250 ml H_2O, 20 ml 70% HNO_3 and 2–3 ml 48% HF for 5 min at 20 °C. To add an alloying element to the surface layer, Nb was predeposited on the polished sample by DC magnetron sputtering of Nb target in argon atmosphere. The thickness of the precoated layer of Nb was controlled at 10 μm to produce an alloyed layer with the same Nb content as that of Zr–2.5 wt% Nb alloy used in CANDU reactors. We assumed that LSM would generate a molten pool about 400 μm thick based on the previous study [11], and a uniform mixing of molten pool with Nb layer could occur during the LSM. Laser processing was conducted using a continuous wave CO_2 laser at a scan rate of 1 m/min with beam power of 2.2 and 2.5 kW, respectively. The final beam at the focal point was 2 mm × 2 mm in size.

The microstructure of laser surface alloyed samples was observed by a polarized optical microscope and a scanning electron microscope (SEM) after swab etching with 20 ml glycerol, 20 ml 70% HNO_3 and 2–3 ml 48% HF solution. The variation of chemical composition in depth of the laser surface alloyed layer was measured by the wave dispersive spectrometer (WDS) equipped in SEM. The structural change of the sample was examined by X-ray diffraction spectrometer (XRD) equipped with a copper target. Hardness of the laser alloyed surface layer was characterized by microindentation. Microhardness depth profiles were obtained from cross-sections of metallographically prepared samples using a Vickers indenter with 200 g loads.

Table 1
Chemical compositions (wt%) of Zircaloy-4

Sn	Fe	Cr	O	Zr
1.32	0.21	0.11	0.122	Balance

The effects of LSA with Nb on the corrosion resistance of Zircaloy-4 were examined in two environments, 4 M NaCl at 80 °C and steam at 400 °C. The effects of LSA with Nb on resistance to the localized corrosion of Zircaloy-4 in the chloride solution were investigated by measuring the pitting potentials that were determined from potentiodynamic polarization curves for the laser surface alloyed samples. The electrochemical cell for anodic polarization tests consisted of a one-liter multineck flask, with platinum counter and saturated calomel reference electrodes positioned in a salt bridge. The anodic polarization tests were performed at a scan rate of 0.5 mV/s in deaerated 4 M NaCl at 80 °C. The solution was deaerated by purging with high-purity nitrogen throughout the tests, starting from 1 h before the tests. In addition, the corrosion resistance of Zircaloy-4, laser surface melted with Nb, were examined by immersion tests under static conditions in 10.3 MPa steam at 400 °C. The samples were hung on a type 304 stainless fixture in an autoclave which permitted total surface exposure to the environment. In accordance with ASTM G2-88, between each test interval samples were removed, air-dried and weighed to determine weight gain. After each weighing, samples were returned to the autoclave.

Hydrogen content was analyzed for as-received and laser surface alloyed samples both before and after corrosion testing. The analysis was performed using a hot extraction method. SEM was used to observe oxide morphologies of as-received Zircaloy-4 and the laser surface alloyed samples exposed to steam at 400 °C.

3. Results and discussion

3.1. Microstructure of laser surface alloyed Zircaloy-4

Fig. 1(a) shows the cross-sectional microstructure of the Nb-deposited Zircaloy-4 observed under polarized lighting condition. The Nb-deposited layer grew in a columnar structure with a thickness of about 10 μm. A laser beam was focused on the pre-Nb deposited samples at beam powers of 2.2 and 2.5 kW, and the resultant microstructures were presented respectively in Fig. 1(b) and (c). An alloyed region near the surface and an interior unalloyed region were identified in the microstructure of the laser treated sample, which was confirmed by WDS. The thickness of the alloyed layer increased from about 170 to 270 μm with increasing the beam power. The microstructure of the layer alloyed at a

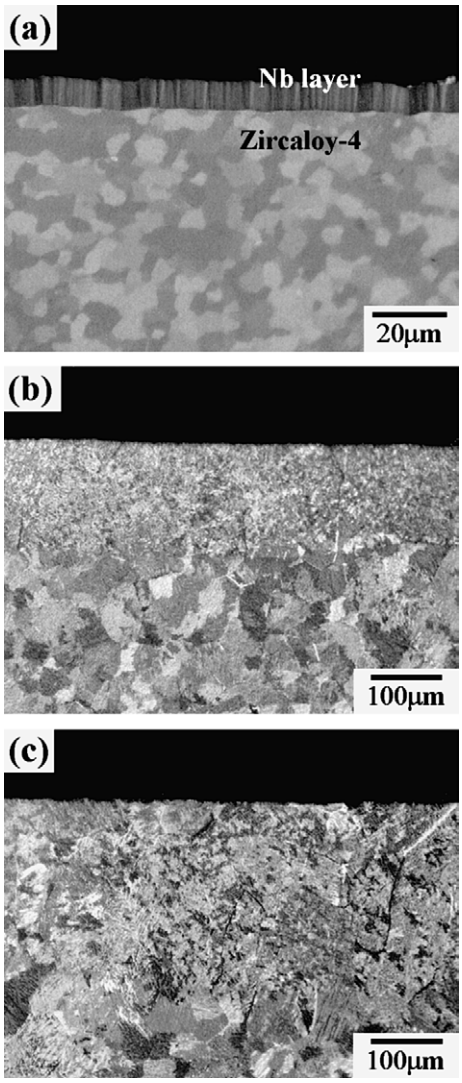

Fig. 1. Optical micrographs showing cross-sections of (a) Nb-coated Zircaloy-4, (b) laser surface Nb-alloyed Zircaloy-4 at 2 kW with a scan rate of 1 m/min, and (c) laser surface Nb-alloyed Zircaloy-4 at 2.5 kW with a scan rate of 1 m/min.

beam power of 2.2 kW became finer than that alloyed at 2.5 kW due to a higher cooling rate at lower beam power. A lower beam power produces a shallower molten pool. A decrease in the molten pool volume enhances heat sink ability via the underlying matrix with increasing the cooling rate.

Fig. 2 shows chemical compositions with depth from the surface of the sample alloyed at different beam powers i.e., 2.2 and 2.5 kW, which were measured by WDS. With an increase in the laser beam power from 2.2 to 2.5 kW, the thickness of the alloyed layer increased from about 200 to 300 μm that is similar to the observation from Fig. 1, while the average Nb content in

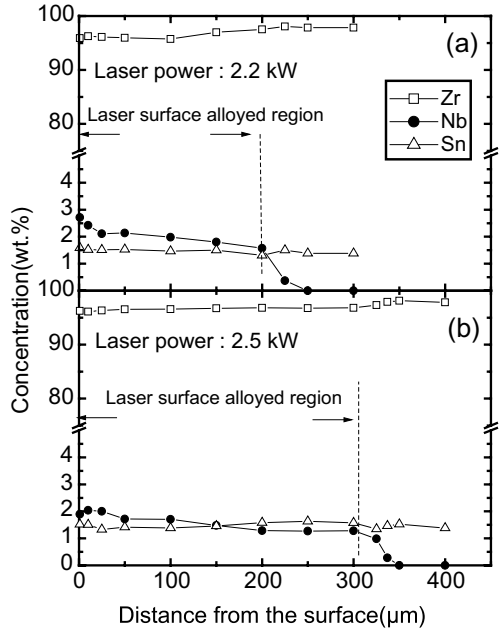

Fig. 2. Concentration profiles measured in depth for laser surface Nb-alloyed Zircaloy-4 (a) at 2.2 kW with 1 m/mm and (b) at 2.5 kW with 1 m/mm.

the alloyed layer decreased. For the sample alloyed at 2.2 kW (Fig. 2(a)), the Nb content of the alloyed layer being more than 2 wt% at 25 μm in depth from surface gradually decreased to 1.57 wt% to a depth of 200 μm. The sample alloyed at 2.5 kW showed a depth profile of Nb content being about 1.7 wt% at 100 μm in depth from the surface, and decreasing to 1.3 wt% at a further depth of 200 μm. The decrease in the Nb content with an increase in the laser power can be attributed to the deeper and greater molten pool formed at higher laser power for a pre-deposited Nb layer with the same thickness. The Nb content in the alloyed layer did not reach the designed level of an average of 2.5 wt%, which is a result of loss of alloying element due presumably to vaporization of deposited Nb during the melting by laser beam.

The XRD patterns of the alloyed Zircaloy-4 revealed that the β-phase of zirconium was newly formed in the alloyed layer due probably to the rapid cooling during the LSA treatment as shown in Fig. 3, whereas only an α-Zr phase (hcp) existed in as-received Zircaloy-4. The β-Zr phase shows body centered cubic (bcc) structure, containing about 18.5 wt% Nb [12]. The addition of Nb to Zr will contribute to the formation of β-Zr phase since the Nb is a β-stabilizer. The intensity of the β-Zr peak increased when laser beam power decreased, as a result of the increased Nb content in the alloyed layer.

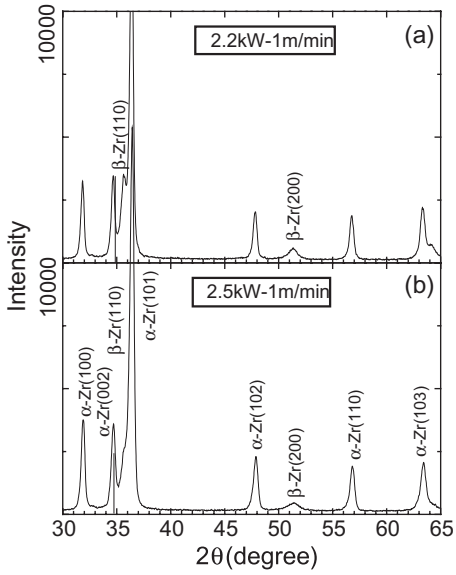

Fig. 3. XRD patterns (θ–2θ scan) of laser surface Nb-alloyed Zircaloy-4 (a) at 2.2 kW with 1 m/mm and (b) at 2.5 kW with 1 m/mm.

3.2. Microhardness of laser surface alloyed Zircaloy-4

Microhardness depth profile of the cross-section of the laser beam treated alloy is shown in Fig. 4. The LSA with Nb increased significantly the hardness of the Zircaloy-4 from 160 Hv for the as received to more than 200 Hv for the laser surface alloyed sample. In particular, the hardness of the alloyed layer increased to the values more than 500 Hv to the depth of 150 μm from the surface. The increase in the hardness of Zircaloy-4 by LSA can be attributed to three factors of LSA, i.e., an alloying with Nb, grain size refinement due to a rapid cooling, and formation of β-Zr phase in the alloyed layer. The slope of ΔHv vs. Nb content plots shown in Fig. 5 increased with a decrease in the beam power from 185 for the sample alloyed at 2.5 kW to 324 for one alloyed at 2.2 kW, though the values became scattered. The difference in the slope of ΔHv vs. Nb content plots is the result of the finer microstructure produced by higher cooling rate at the lower beam power as shown in Fig. 1. In addition, the increase in hardness of the laser surface alloyed layer was also attributed partially to the formation of β-Zr phase accompanying with volume expansion as discussed in the previous section. The increase in the microhardness due to the LSA may improve the wear resistance of Zircaloy-4.

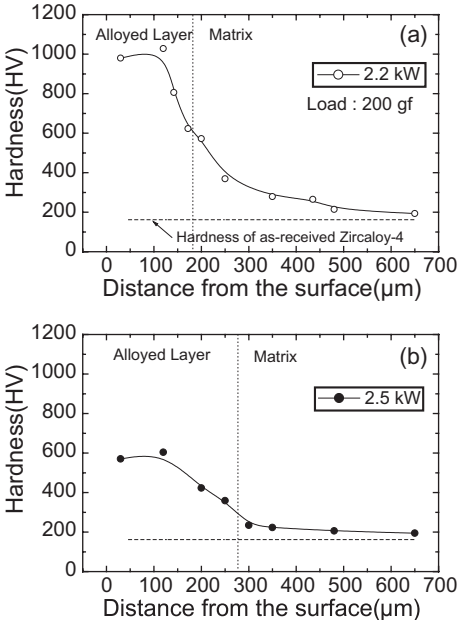

Fig. 4. Microhardness measured on cross-section of laser surface Nb-alloyed Zircaloy-4 (a) at 2.2 kW with 1 m/mm and (b) at 2.5 kW with 1 m/mm.

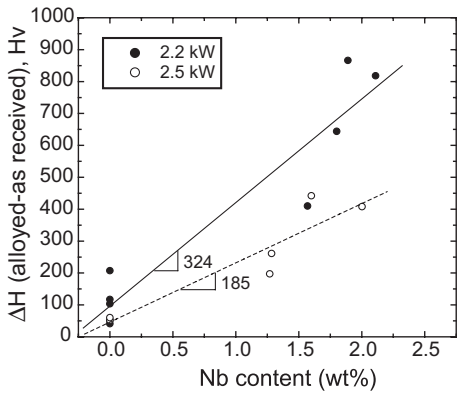

Fig. 5. Hardness variation with Nb content in laser surface Nb-alloyed Zircaloy-4.

3.3. Corrosion behavior of laser surface alloyed Zircaloy-4 in a chloride solution

Fig. 6 shows the effect of Nb alloying on the anodic response of Zircaloy-4 in deaerated 4 M NaCl solution at 80 °C. The resistance to localized corrosion of the laser surface alloyed layer was enhanced as indicated by the increase in pitting potential from 350 mV for the as-received to about 1200 mV for the laser alloyed samples. However, the influence of laser beam power on the corrosion resistance was not clearly shown unlike on the hardness. Since LSA brings about three distinct effects, i.e., the fine microstructure, the formation of β-Zr phase, and the alloying with Nb, independent effects of the LSA and the alloying with 2.5 wt% Nb on the anodic polarization response of the alloys were examined by comparing them with that of as-received Zircaloy-4. Fig. 7

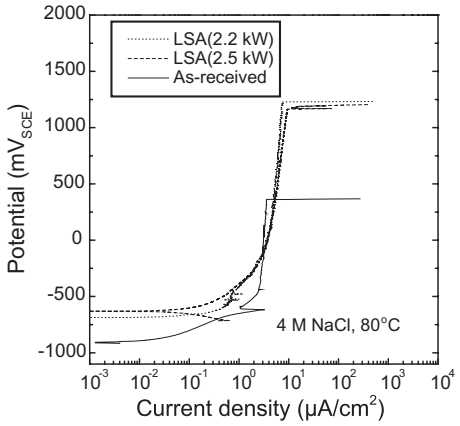

Fig. 6. Anodic polarization curves of as-received Zircaloy-4 and laser surface Nb-alloyed Zircaloy-4 in deaerated 4 M NaCl at 80 °C.

shows the anodic polarization responses for the laser surface melted Zircaloy-4 without alloying with Nb, as-received Zr–2.5% Nb alloy, and as-received Zircaloy-4 in deaerated 4 M NaCl solution at 80 °C. As-received Zr–2.5% Nb alloy is composed of a mixed structure of α-Zr and β-Zr. The pitting potential for each alloy exhibited significantly different value; 720 mV for the laser surface melted Zircaloy-4 without alloying with Nb, 650 mV for the as-received Zr–2.5% Nb alloy and 350 mV for the as-received Zircaloy-4. Thus, it appears that the improvement of resistance to localized corrosion by the LSA with Nb, shown in Fig. 6, was attributed to the combined effects of the rapidly cooled fine microstructure, the formation of β-Zr phase and the alloying with Nb. Generally, grain boundaries are more susceptible to corrosion compared with grain interior due to impurities concentrated at grain boundaries during solidification of metals [13,14]. LSM can reduce the amount of the defects at the grain boundaries due to a rapid cooling after melting, and consequently increase the corrosion resistance of the laser surface melted layer although the layer has numerous grain boundaries. Banikel et al. [15] explained that LSM improved the corrosion resistance of stainless steel AISI 321 and aluminum alloy AA6082 in a chloride solution by eliminating preferential sites for pit formation such as precipitates and inclusions; small noncrystallographic shallow pits formed and uniform corrosion attack occurred on the laser surface melted layer of aluminum alloy due to an ultra-fine microstructure.

3.4. Corrosion behavior of laser surface alloyed Zircaloy-4 in steam

Corrosion kinetics for the laser surface alloyed Zircaloy-4 was measured in steam at 400 °C and is presented in Fig. 8, along with that for the as-received sample. While the LSA with Nb improved the corrosion resistance of Zircaloy-4 in chloride solution at low temperature as shown in Fig. 7, it did not enhance the corrosion resistance of the alloy in steam at 400 °C. The LSA treated samples exhibited higher corrosion rates compared with that of the as-received sample, and the alloyed sample at 2.2 kW showed higher corrosion rate than the alloyed sample at 2.5 kW. As discussed in the previous section, these effects of LSA can probably be considered in three factors of LSM; Nb alloying, fine microstructure and formation of β phase. The fine microstructure due to LSM apparently did not affect corrosion resistance of the alloy in steam, as shown in Fig. 8. It was reported that Zr–2.5% Nb alloy with the β-Zr phase showed poor corrosion resistance in the D_2O steam [16] and H_2O steam at 400 °C [17]; Zr–2.5% Nb

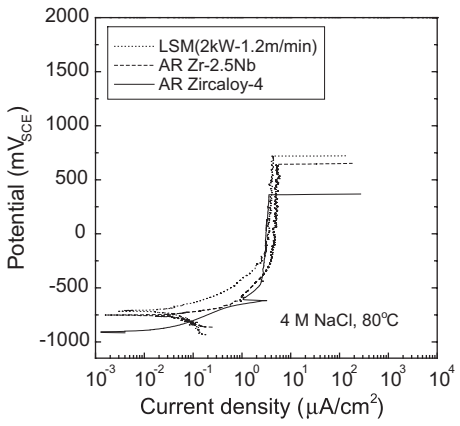

Fig. 7. Anodic polarization curves of laser surface melted Zircaloy-4, as-received Zr–2.5% Nb, and as-received Zircaloy-4 in deaerated 4 M NaCl at 80 °C.

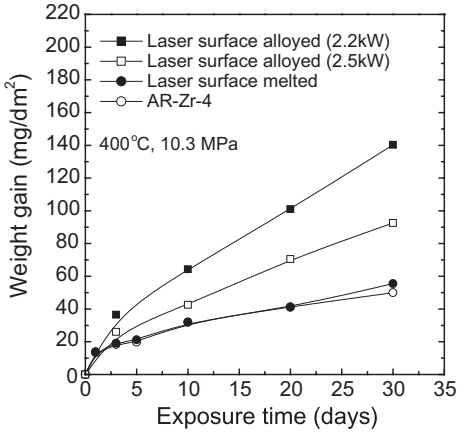

Fig. 8. Weight gain vs. exposure time for as-received Zircaloy-4, laser surface treated Zircaloy-4, and laser surface Nb-alloyed Zircaloy-4 in steam at 400 °C.

with a mixed structure of α-Zr and β-Zr exhibited the weight gain of about 90 mg/dm^2 that is almost 2 times higher than the as-received Zircaloy-4 (50 mg/dm^2) after exposure to steam at 400 °C for 30 days. It is not yet fully understood how β-Zr phase decreases the corrosion resistance of Zr–Nb alloy in high temperature water or steam. Choo et al. [16] explained that the instability of β-Zr phase is one reason for this decrease in corrosion resistance. Another plausible reason is that the β-Zr with bcc structure shows an open structure compared with α-Zr with hcp structure, and hence oxygen and hydrogen easily diffuse through the β-Zr. Therefore, the decrease in corrosion resistance of Zircaloy-4 alloyed with Nb may be associated with the β-Zr phase formed in the alloyed layer. Higher corrosion rate of the sample alloyed under low beam power results from the greater amount of the β-Zr phase in the alloyed layer with higher Nb content, as shown in Fig. 3.

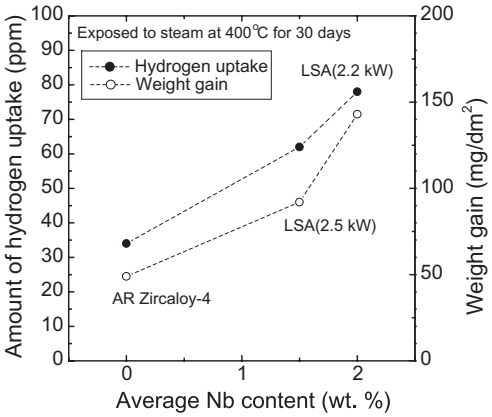

Fig. 9. Effect of Nb content on hydrogen uptake and weight gain for laser surface alloyed Zircaloy-4, exposed to steam for 30 days at 400 °C.

Hydrogen uptake for the sample exposed to steam was measured, and presented in Fig. 9. The sample alloyed at 2.2 kW exhibited the highest amount of hydrogen uptake, followed by the alloyed sample at 2.5 kW, and then the as-received sample. This is the same order as that for weight gain of the samples. Fig. 10(a) and (b) are SEM micrographs showing the cross-sections of both the as-received and the LSA treated samples after exposure to steam at 400 °C for 30 days. The oxide formed in the as-received sample had few defects, whereas the oxide formed in the laser surface alloyed sample had many defects such as lateral microcracks. The defect density was increased with a decrease in beam power (i.e., with an increase in amount of β-Zr), as shown in Fig. 11. It appears that the cracks were formed during the sample preparation for the microscopic

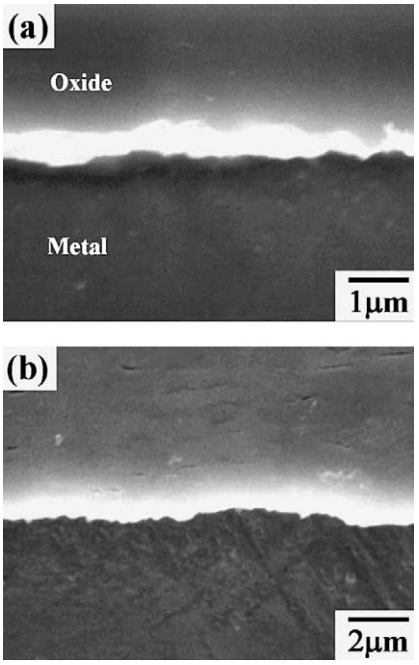

Fig. 10. SEM micrographs showing cross-section of as-received Zircaloy-4 and laser surface alloyed Zircaloy-4 after 30-day test in a steam at 400 °C. Swab etched in 20 ml glycerol, 20 ml 70% HNO_3, and 2–3 ml 48% HF: (a) as-received Zircaloy-4, (b) laser surface Nb-alloyed Zircaloy-4 with power of 2.5 kW.

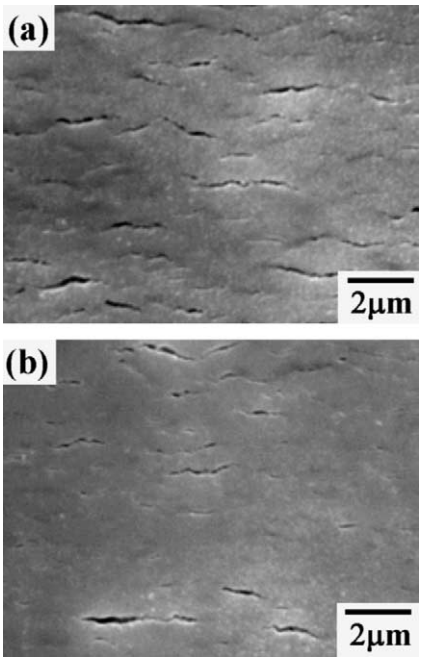

Fig. 11. SEM micrographs showing cracks formed on the surface oxide of laser surface Nb-alloyed Zircaloy-4 after 30-day test in steam at 400 °C: (a) Nb-alloyed at power of 2.2 kW, and (b) Nb-alloyed at power of 2.5 kW.

observation because the cracks were not observed on an unpolished surface. Figs. 10 and 11 shows that the oxide formed on the laser-alloyed sample is brittle, which may be attributed to precipitation of Zr hydride. Hydrogen uptake of LSA samples is 1.8–2.3 times higher than that of the as-received as shown in Fig. 9. The β-Zr phase formed in the LSA treated layer increased the corrosion reaction ($Zr + 2H_2O \rightarrow ZrO_2 + 4H$) rate, leading to the increase in the amount of hydride that accelerated the corrosion rate of laser-alloyed Zircaloy-4.

Recent studies have shown that the corrosion of Zircaloy-4 is accelerated by the precipitation of hydride [18,19]. Garde [18] suggested adverse effects of hydride precipitation in mechanical aspects: mechanical breakdown of barrier oxide layer due to the hydride precipitation, and fracture at the metal–oxide interface enhances the corrosion rate.

4. Conclusions

(1) LSA on the Zircaloy-4 produced a Nb-alloyed layer 170–300 μm thick with 1.3–2.5 wt% Nb, depending on laser beam power. With increasing laser beam power, Nb content in the alloyed layer was decreased due to the deeper and greater molten pool formed at higher laser power for a pre-deposited Nb layer with a constant thickness. The alloyed layer was composed of a mixed structure of α-Zr and β-Zr phases with the β-Zr phase being increased with the Nb content in the alloyed layer.

(2) LSA increased the microhardness of Zircaloy-4, which was attributed primarily to the three factors; the grain-size refinement by rapid cooling, the solid solution hardening with Nb, and the formation of transformed β phase.

(3) The resistance to localized corrosion of Zircaloy-4 in a chloride solution was significantly improved by LSA with Nb, which was attributed to the combined effects of fine rapidly cooled microstructure and Nb alloying.

(4) LSA with Nb reduced the corrosion resistance of Zircaloy-4 in steam at 400 °C, which appeared to be associated with the β-Zr phase and Zr hydrides.

Acknowledgements

This work was done under '97 Nuclear R&D supported by Korean Ministry of Science and Technology and '97 Electrical Technique Research supported by Electrical Engineering & Science Research Institute.

References

[1] J.C. Clayton, R.L. Fisher, Proc. ANS Topical Meet on Light Water Reactor Fuel Performance, FL, USA, 1985, p. 3.1.
[2] E.H. Novendstern, Meetings on Fuel Performance, KEP-CO/KINS/Westinghouse, 1994.
[3] G.P. Sabol, G.R. Klip, M.G. Balfour, E. Roberts, in: L.F.P. Van Swan, C.M. Eucken (Eds.), Proc. 8th Int. Symp. on Zirconium in the Nuclear Industry, ASTM STP 1023, ASTM, Philadelphia, 1989, p. 227.
[4] A.V. Nikulina et al., in: E.R. Bradley, G.P. Sabol (Eds.), Proc. 11th Int. Symp. on Zirconium in the Nuclear Industry, ASTM STP 1295, ASTM, Philadelphia, 1996, p. 785.
[5] R.J. Comstock, G. Schoenberger, G.P. Sabol, in: E.R. Bradley, G.P. Sabol (Eds.), Proc. 11th Int. Symp. on Zirconium in the Nuclear Industry, ASTM STP 1295, ASTM, Philadelphia, 1996, p. 711.
[6] W. Kim, K.S. Jung, B.H. Choi, H.S. Kwon, S.J. Lee, J.G. Han, M.I. Guseva, Surf. Coat. Technol. 76&77 (1995) 595.
[7] G. Tang, B.H. Choi, W. Kim, K.S. Jung, H.S. Kwon, S.J. Lee, J.H. Lee, T.Y. Song, D.H. Shon, J.G. Han, Surf. Coat. Technol. 89 (1997) 252.
[8] S.J. Lee, H.S. Kwon, W. Kim, B.H. Choi, Mater. Sci. Eng. A 263 (1999) 23.
[9] W. Reitz, J. Rawers, Surface Modification Technology IV, TMS, Philadelphia, 1991, p. 349.
[10] W. Reitz, J. Rawers, J. Mater. Sci. 27 (1992) 2437.
[11] H.S. Kwon, S.J. Lee, A Study on the Improvement of Corrosion Resistance of Fuel Cladding Material by Surface Modification, EESRI 97-015, Korea, 1998.
[12] J.P. Abriata, J.C. Bolcich, Bull. Alloy Phase Diag. 3 (1982) 1710.
[13] D.M. Follstatedt, Laser, Electron-Beam Interactions with Solids, MRS Symp. Proc., Pittsburgh, Penn, 1981, p. 377.
[14] D.L. Piron, The Electrochemistry of Corrosion, NACE International, Houston, TX, 1991, p. 81.
[15] J. Barnilkel, T. Seefeld, A. Emmel, E. Schubert, H.W. Bergmann, JOM 48 (1996) 29.
[16] K.N. Choo, Y.H. Kang, S.I. Pyun,, V.F. Urbanic, J. Nucl. Mater. 209 (1994) 226.
[17] K.N. Choo, S.C. Chul, Y.S. Kim, Korean J. Mater. Sci. 8 (1998) 3.
[18] A.M. Garde, in: C.M. Eucken, A.M. Garde (Eds.), Proc. 9th Int. Symp. on Zirconium in the Nuclear Industry, ASTM STP 1132, ASTM, Philadelphia, 1991, p. 566.
[19] M. Blat, D. Noel, in: E.R. Bradley, G.P. Sabol (Eds.), Proc. 11th Int. Symp. on Zirconium in the Nuclear Industry, ASTM STP 1295, ASTM, Philadelphia, 1996, p. 319.